3D quantification of viral transduction efficiency in living human retinal organoids

Teresa S. Rogler[1,2], Katja A. Salbaum[1,2], Selina M. Sonntag[1], Rebecca James[1], Elijah R. Shelton[1], Achim T. Brinkop[1], Thomas Klopstock[3,4,5], Sabrina Babutzka[2,6], Stylianos Michalakis[2,6], Friedhelm Serwane[1,2,3]

[1]Faculty of Physics and Center for NanoScience (CeNS), LMU, Munich, Germany

[2]Graduate School of Systemic Neuroscience (GSN), Munich, Germany

[3]Munich Cluster for Systems Neurology (SyNergy), Munich, Germany

[4]Friedrich Baur Institute at the Department of Neurology, University Hospital, LMU Munich, Germany

[5]German Center for Neurodegenerative Diseases (DZNE), Munich, Germany

[6]Department of Ophthalmology, LMU Hospital, LMU Munich, Munich, Germany

Keywords: Retina organoids, Gene therapy, Adeno-associated virus, 3D segmentation

Abstract

The development of therapeutics relies on testing their efficiency and specificity in animals and human *in vitro* models. To optimize the efficiency of a gene therapy, for example, fluorescent reporters expressed by treated cells are often utilized as readouts. Traditionally, the overall fluorescence signal provides an estimate for the global transduction efficiency. However, detailed analysis of the transduction efficiency in individual cells within a tissue remains a challenge. Readout on a single cell level can be realized via fluorescence-activated cell sorting at the cost of tissue dissociation into single cells and loss of spatial information. Complementary, spatial information is accessible via immunofluorescence characterization of fixed samples. However, those approaches impede time-dependent studies and prevent the recording of the dynamic interplay between the viral vector and the target cells in a 3D tissue.

Here, we provide a quantitative, three-dimensional characterization of viral transduction efficiencies in living retinal organoids. We combine engineered adeno-associated virus (AAV) vectors, confocal live-imaging, and deep learning-based image segmentation to establish a quantitative test platform for gene delivery. To establish this, we transduced human retinal organoids with specific AAV vectors and imaged the fluorescent reporter expression in 3D. We measured a faster onset (7 days) and higher transduction efficiency (82%) of an AAV vector with optimized serotype (AAV2.NN) compared to two other AAV serotypes (AAV2.7m8, AAV9.NN). This highlights the practicality and functionality of our platform as a testbed for future treatments. The combination of optimized viral vectors, live-imaging, and deep learning-based image processing has the potential to guide the development of therapies in a variety of biomedical applications.

Introduction

Development of advanced therapeutics builds on years of *in vitro* and animal research. A prime example is the development of retinal gene therapies based on AAV vectors which have led to several clinical programs and one gene therapy product approval (1,2).

Human retinal organoids (hROs), which are stem cell-derived *in vitro* models for human retinal tissue, are an emerging model system that has the potential to transform preclinical drug testing (3–5). State-of-the-art protocols enable the culturing of hROs that possess tissue-specific cell types, morphological characteristics of the neural retina (NR), and the retinal pigment epithelium (RPE). hROs display light sensitivity and synaptic connectivity (6–10). Due to their physiological relevance hROs enable insights into the mechanisms behind retinal development (11,12) and diseases (13). Recent studies used hROs to test and optimize mRNA

delivery via liposomes (14) and gene delivery via AAV vectors (1,2,15–17). Now, they are emerging as a complementary *in vitro* system for gene therapy testing (18,19).

Transduction efficiency of novel AAV vectors is typically assessed with vector genomes coding for fluorescent proteins. The fluorescence expression is then used as an indicator for the vector's ability to transduce cells. Traditionally, estimates of transduction efficiencies were either obtained by recording fluorescence levels without further quantification (2), normalizing the overall fluorescence level of a whole organoid to that of a constitutive nuclear stain like DAPI (16), or comparing the overall fluorescence level obtained with different vectors without normalization (15). These approaches face the fundamental challenges that a single, strongly transduced cell cannot be distinguished from multiple transduced cells with low fluorescence level (Fig. 1). This ambiguity makes the assessment of the viral vector efficiency difficult. To quantify transduction on a single cell level, fluorescence-based FACS (Fluorescence Activated Cell Sorting) analysis (17) can be performed. However, due to the requirement of organoid dissociation, the spatial information is lost and signals from non-retinal tissue as found in retinal organoids (6) could not be excluded from the single-cell pool. To access spatial transduction information, researchers typically use fixed samples (20) which limits readout of critical information that can be gained through longitudinal studies.

Here, we introduce 3D quantification of AAV transduction efficiency in living retinal organoids with single-cell resolution (Fig. 1). To sample the entire retinal cross section of living hROs we imaged their retinal part using confocal microscopy (Fig. 1A). The segmentation of individual neurons in a densely packed tissue typically requires super-resolution microscopy which poses severe challenges to the imaging hardware (21). To lower the hurdle, we focused on the segmentation of the overall transduced volume instead of separation of

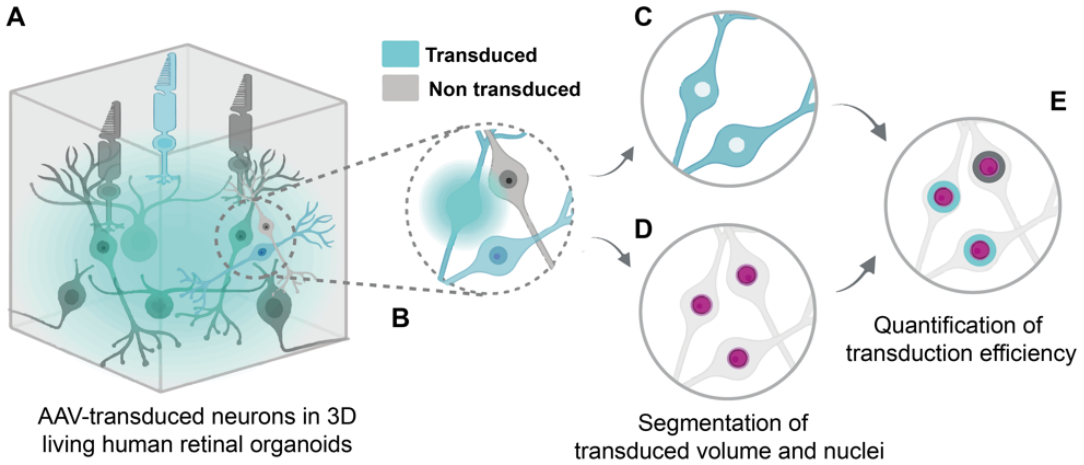

Figure 1. Quantification of viral vector transduction efficiencies in living human retinal organoids. (A) Cells are densely packed and (B) show varying expression levels if transduced. A quantitative measure of the transduction efficiency is obtained by segmentation of the transduced volume (C) via machine learning and of the nuclei (D) via deep learning techniques (22). Transduced cells are classified by evaluating the transduction segmentation within a thin virtual shell around each nucleus (E).

individual cells. To classify this volume independently of the fluorescence signal intensity of the individual neurons, we use a machine learning algorithm which we trained with a minimal set of data consisting of transduced cells with varying brightness (Fig. 1C, see Methods). To segment cell nuclei, we used the deep learning-based segmentation software Cellpose (Fig. 1D) due to its performance in dense tissues (22). To evaluate whether a cell was transduced, we quantified the overlap of a thin shell covering each nucleus with the transduced volume (Fig. 1E). We used our pipeline to test 3 AAVs with different capsids (AAV2.7m8, AAV9.NN, AAV2.NN), and tracked their transduction efficiency spatially over a period of 40 days with 4 individual time points. The ability to quantify transduction efficiencies in living organoids allows viral vector evaluation and optimization in human retinal tissue. Moreover, it opens the door to spatially resolved longitudinal studies for any delivery experiment involving cytoplasmic fluorescent reporters.

Results

Culture of human retinal organoids

Human retinal organoids were grown following the protocol from Cowan et al. with minor adjustments ((6), see Methods). First, iPSCs were passaged and plated onto Matrigel-coated plates. To induce the formation of embryoid bodies (Fig. 2A), cells were resuspended and seeded into agarose wells. Throughout organoid growth, medium was replaced according to a defined schedule (see Methods). To induce the formation of the eye field, the embryoid bodies were transferred to Matrigel-coated plates on day 7 (Fig. 2B). On day 31,

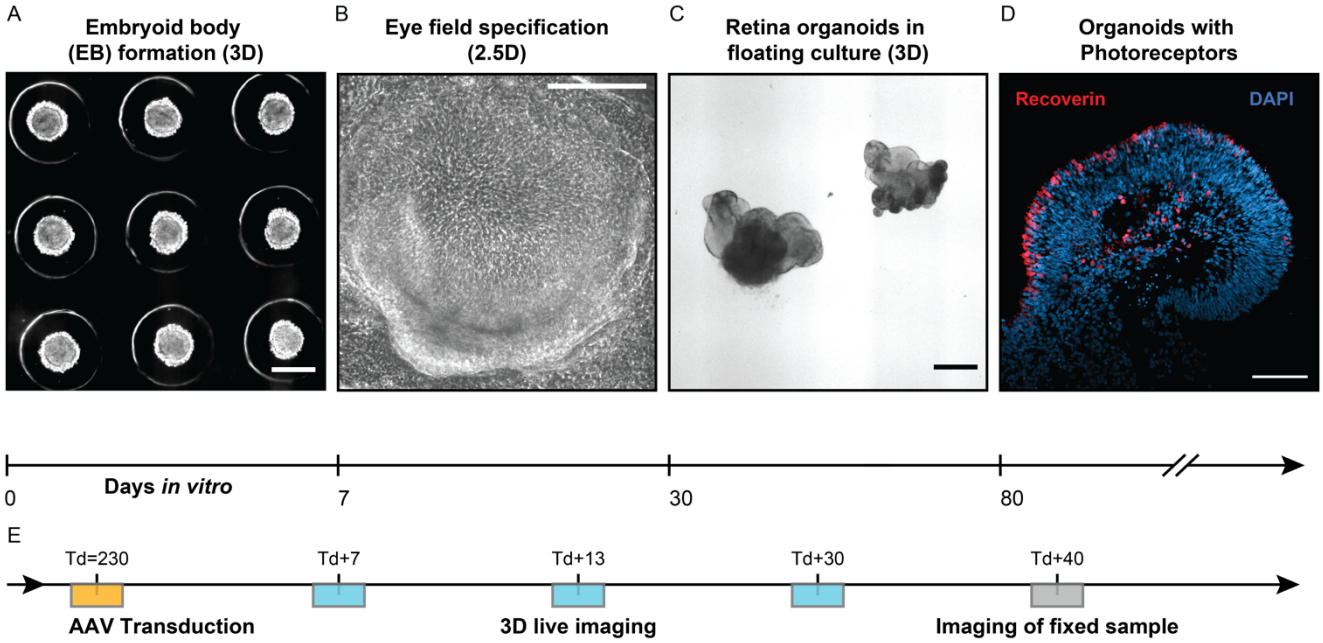

Figure 2. Human retinal organoids as a test bed for viral transduction. (A) Induced pluripotent stem cells (iPSCs) were transferred to 3D culture to form embryoid bodies (EB). (B) Re-plating the EBs onto 2D geometry while supplying specific biochemical signals triggered the specification of the eye field (see Methods). (C) Floating culture enabled cell differentiation of retinal cell types. (D) 80 days old organoids displayed photoreceptor cells. (E) Transductions were carried out around DIV230 (yellow). Living transduced organoids were imaged and fixed 40 days after transduction (Td+40). Image types: (A-C) Brightfield, (D) immunofluorescence. Scale bars (A-C) 500µm, (D): 100µm.

retinal structures were detached to obtain floating cultures while organoids without neuroepithelium were removed (Fig. 2C). To facilitate retina maturation, the medium was supplemented with FBS and taurine at day 42, and with retinoic acid at day 70. From day 98 onwards, the medium was modified with N-2 supplement and reduced retinoic acid concentration. The human retinal organoids obtained were subsequently characterized using immunofluorescence. Hereby photoreceptor cells (Fig. 2D) as well as various retina cell types (Suppl. Fig. S5) were observed.

AAV transduction of human retinal organoids

To demonstrate our approach, we transduced human retinal organoids with 3 adeno-associated viral vectors with different serotypes. In addition to using clinically tested serotype AAV2.7m8 (23) as a control, two optimized serotypes were selected. Serotypes AAV2 and AAV9 have been previously reported to enhance the transfer of genetic material to retinal cells (16). An engineered version of AAV2 (AAV2.NN) was used due to its superior performance compared to AAV2.7m8 with respect to transduction efficiency and onset kinetics (24). AAV9.NN is a modified AAV9 variant carrying the peptide insertion of AAV2.NN. Potential clinical applications may benefit from testing in as mature human retinal tissue as possible; thus, we transduced hROs which were Td = 230 days old (Fig. 2). Each organoid was supplied with $5*10^{10}$ vector genomes (see

Methods). Eight hROs were transduced at consecutive days centred at Td = 230(-3, +4) days (Fig. 2E, yellow box), imaged at three timepoints Td+7, Td+13, Td+30, and fixed at Td+40 (Fig. 2E, grey box).

Confocal 3D live imaging

To obtain 3D images of the nuclei (Fig. 3A) as well as of the AAV-induced eGFP fluorescence, (Fig. 3A) a commercial confocal microscope (Zeiss LSM980) was used in combination with a 40x water immersion objective. The height of the observation volume was chosen to cover the entire retinal cross-section of 100µm depth. All measurements were taken using this standardized imaging volume. An experimental hurdle for imaging in deeper retinal layers is the wavelength-dependent penetration depth of the laser light which can be increased e.g. using a 2-photon excitation source (25). We overcame this problem by using a near-infrared

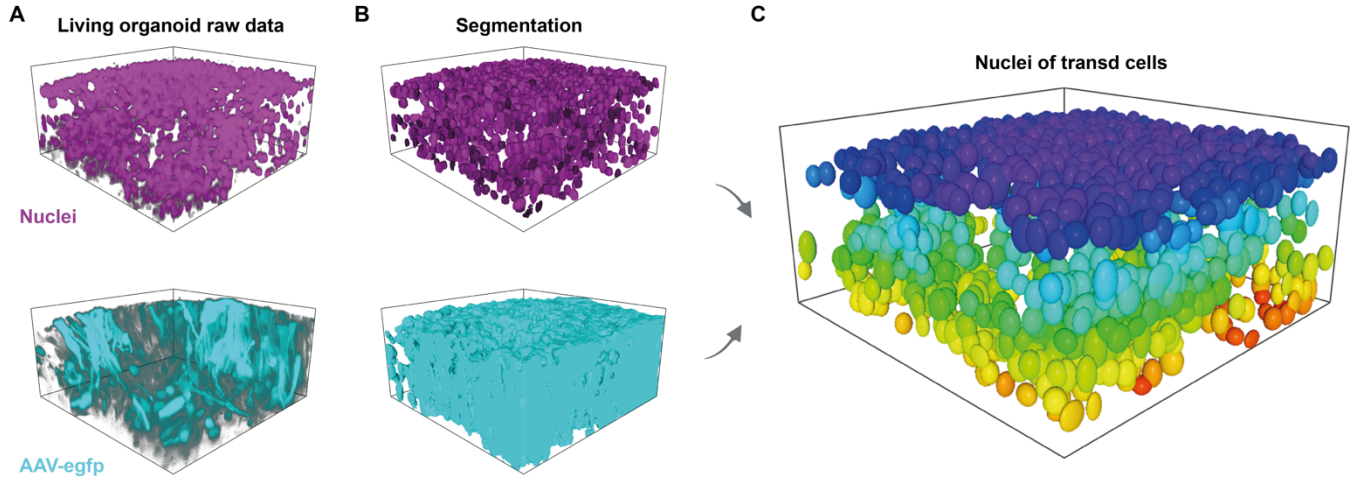

Figure 3. Quantification of transduction efficiency in living human retinal organoids. (**A**) Raw confocal image of 241-day old human retinal organoid transduced with AAV2.NN. (**B**) Segmentation of nuclei via deep learning (22) and transduced volume via machine learning (see Methods). (**C**) Nuclei of transduced cells - elliptical approximation. Colour coding according to z-position. Observation volume b x w x h: 211x211x100 μm^3.

dye for the nuclei staining (excitation wavelength: 650nm, see Methods) and increasing the laser intensity with respect to imaging depth (see Methods). Accordingly, the illumination intensity was adjusted to saturate 1-2 cells within each imaging plane. A 3D rendering of the raw data can be seen in Fig. 3A.

3D Segmentation and quantification of transduction efficiency

The transduction efficiency is defined as $E = N_{Td} / N_{Tot}$ where N_{Td} is the number of transduced cells and N_{Tot} the total cell number, respectively. Obtaining N_{Td} from 3D live confocal microscopy images of cytoplasmic reporters is challenging for human retinal organoids, but also for other neuronal tissues: Cells are densely packed, substantially vary in aspect ratio and in fluorescence intensity due to cell type specific expression and transduction. To overcome this problem, we used a 3 step approach: First, we obtained N_{Tot} as well as positional information of all neurons by segmenting all nuclei using the deep learning software Cellpose (22) (Fig. 3B). This eliminated the requirement to distinguish single neurons in the harder-to-segment cytoplasmic channel.

In a second step we segmented the transduced volume. In previous fluorescent-based approaches, the overall fluorescence was used as a proxy for the transduction efficiency (17). When the transduction efficiency is evaluated in this way, few transduced bright cells and many transduced cells with low fluorescence intensity yield the same result (Fig. 1B). To overcome this ambiguity, we trained a machine learning algorithm on both low and high cytoplasmic intensity fluorescence signals (Fig 3B, see Methods). In a last step we evaluated whether a neuron was transduced. For this we calculated the overlap between a thin virtual shell (thickness 0.8 µm) surrounding each nucleus with the segmentation of the transduced volume. When 40% or more of the shell contained transduced volume, the cell was considered transduced. The

threshold was determined by comparing the algorithm's transduction efficiency with the efficiency obtained by three human annotators (Suppl. Fig. S1).
We then used our pipeline to quantify the transduction efficiency in living hRO with 3 different AAV serotypes AAV2.7m8, AAV2.NN and AAV9.NN (Fig. 4) at 3 different time points. At a fourth timepoint, (Td+40), the organoids were fixed. The transduced nuclei's ellipsoidal approximations are rendered in Fig. 4B and the

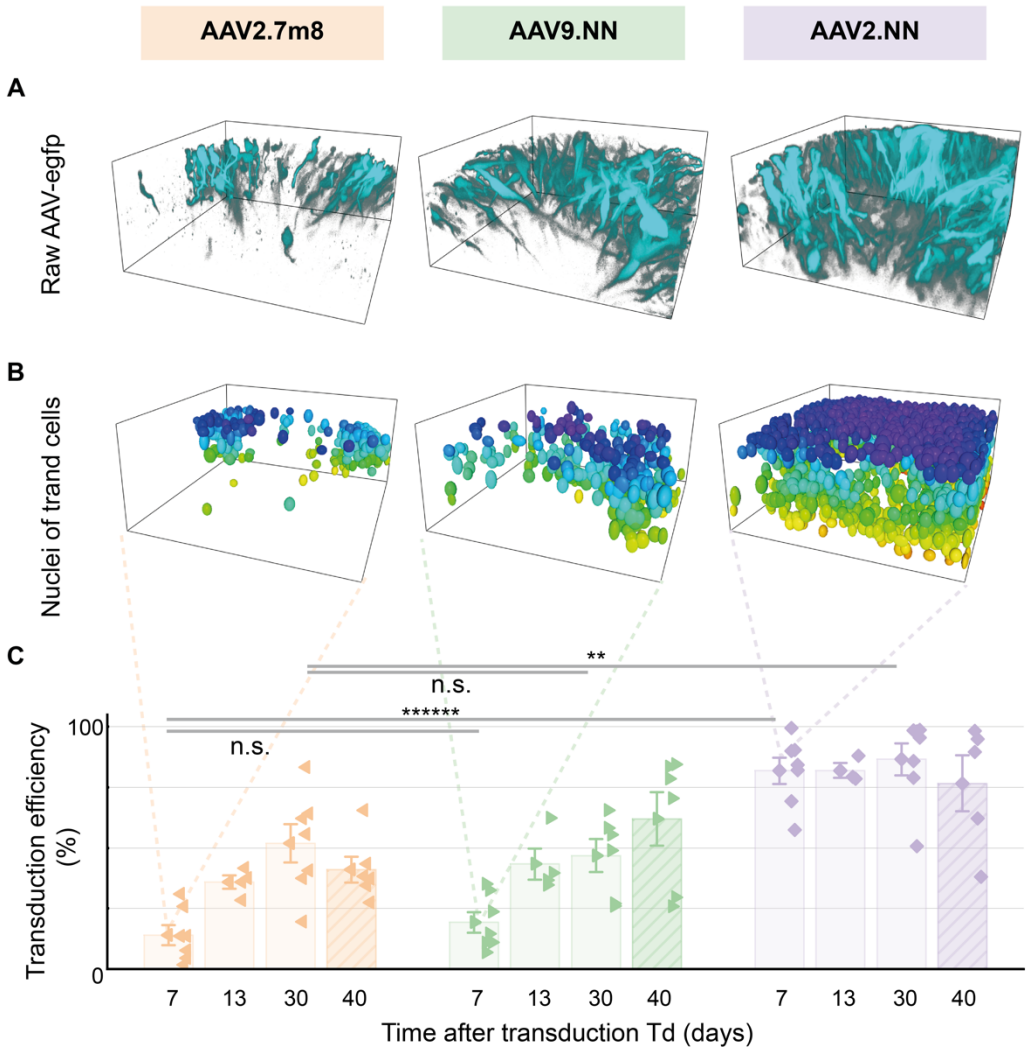

Figure 4. Transduction efficiency quantification for AAV serotypes AAV2.7m8 AAV2.9NN and AAV2.NN. (A) Representative raw images of living retina organoid 7 days after transduction. (B) Elliptical approximations of nuclei of transduced cells from (A). (C) Transduction efficiency. AAN2.NN has a faster onset and a higher overall efficiency compared to AAV2.7m8 and AAV2.9NN. AAV2.7m8: N = (7,4,7,6); AAV9.NN: N = (7,4,6,6); AAV2.NN: N = (7,3,7,5) for (Td+7, Td+13, Td+30, Td+40). Td+7-Td+30: living organoids; Td+40: fixed organoids (see Methods). Error bars indicate the standard error of the mean (SEM).

means and standard errors for the transduction efficiency $E = N_{Td} / N_{Tot}$ for all samples are plotted in Fig. 4C. The results obtained from living organoid samples (Td+30) agreed with the fixed samples (Td+40) within the error bars, indicating that fixed, whole mount organoids yield comparable results to our live imaging approach (shaded bars). As a negative control, untreated wildtype organoids were used. As a positive control we imaged and analysed transgenic mouse retinal organoids endogenous eGFP expression under control of the *Rax* (rx) promotor (25). For the negative control we obtained eGFP expression of 0% while the positive control showed eGFP expression in 99.9% of cells (Suppl. Fig. S1), highlighting the broad dynamic range of our approach. One week after transduction (Td+7) we observed a difference in efficiency between the tested serotypes AAV2.7m8, AAV9.NN and AAV2.NN (Fig. 4A). While serotypes AAV2.7m8 and AAV9.NN showed a similar onset time and overall level of eGFP expression, serotype AAV2.NN outperformed the other two variants substantially. Our work recovers the fast onset time of less than 7 days in transduction experiments

performed with AAV2.NN (16) as well as significant higher transduction efficiency found with AAV2.NN when compared to AAV2.7m8 7 days post viral introduction (15). Most importantly, we can pinpoint the absolute number of transduction efficiency, which amounts to (82 ± 5) % of the cells within the retinal organoid in the case of AAV2.NN (Td+7).

Discussion

In summary, we developed an imaging and segmentation pipeline for intact living human retinal organoids. We performed live imaging of eGFP-expressing transduced cells and stained nuclei in an observation volume which captures the entire retinal cross-sections containing thousands of cells. Combining deep learning for the robust segmentation of nuclei and a machine learning algorithm which requires a minimal set of training for transduced cells, we have direct access to the total number of transduced cells, spatially resolved. We used the platform to quantify AAV transduction efficiency of three different serotypes. With the goal to enable longitudinal imaging of living samples, we quantified the transduction efficiency as a function of time, up to 40 days. We found that AAV2.NN outperforms the serotypes AAV9.NN and AAV2.7m8 with respect to onset time and overall efficiency.

One key advantage of our approach is the accessibility of 3D spatial-temporal information of transduction. Existing techniques were limited to fixed samples (16,20) or FACS analysis (17), preventing longitudinal studies; alternatively the overall fluorescence was assessed at the cost of spatial information (15). Aside from the methodological benefits, the implementation hurdles are lower when compared to existing approaches. The application only requires a standard confocal microscope and time-consuming whole mount imaging or cryo-sectioning can be avoided by allowing longitudinal imaging. While the approach has been optimized to work with densely packed tissue, adaption of the nuclei shell overlap threshold might be required when used in tissues with different cell densities.

The technology introduced here can be readily used in other organoid systems, both neuronal such as brain organoids and non-neuronal. It could be expanded to organ explants including retina explants and brain slices. More broadly, it will leverage efficiency and specificity quantification of other transfection techniques in a spatiotemporal way, such as mRNA delivery (14) and nanoparticles (26), thereby improving the development of therapies.

Bibliography

1. Buck TM, Wijnholds J. Recombinant Adeno-Associated Viral Vectors (rAAV)-Vector Elements in Ocular Gene Therapy Clinical Trials and Transgene Expression and Bioactivity Assays. Int J Mol Sci. 2020 Jan;21(12):4197.
2. Tornabene P, Trapani I, Minopoli R, Centrulo M, Lupo M, de Simone S, et al. Intein-mediated protein trans-splicing expands adeno-associated virus transfer capacity in the retina. Sci Transl Med. 2019 May 15;11(492):eaav4523.
3. Nakano T, Ando S, Takata N, Kawada M, Muguruma K, Sekiguchi K, et al. Self-Formation of Optic Cups and Storable Stratified Neural Retina from Human ESCs. Cell Stem Cell. 2012;
4. Zhong X, Zhong X, Gutierrez C, Xue T, Hampton C, Vergara MN, et al. Generation of three-dimensional retinal tissue with functional photoreceptors from human iPSCs. Nat Commun. 2014;
5. Capowski EE, Samimi K, Mayerl SJ, Phillips MJ, Pinilla I, Howden SE, et al. Reproducibility and staging of 3D human retinal organoids across multiple pluripotent stem cell lines. Dev Camb Engl. 2019 Jan 9;146(1):dev171686.
6. Cowan CS, Renner M, De Gennaro M, Gross-Scherf B, Goldblum D, Hou Y, et al. Cell Types of the Human Retina and Its Organoids at Single-Cell Resolution. Cell. 2020 Sep 17;182(6):1623-1640.e34.
7. Dorgau B, Felemban M, Hilgen G, Kiening M, Zerti D, Hunt NC, et al. Decellularised extracellular matrix-derived peptides from neural retina and retinal pigment epithelium enhance the expression of synaptic markers and light responsiveness of human pluripotent stem cell derived retinal organoids. Biomaterials. 2019 Apr 1;199:63–75.
8. Hallam D, Hilgen G, Dorgau B, Zhu L, Yu M, Bojic S, et al. Human-Induced Pluripotent Stem Cells Generate Light Responsive Retinal Organoids with Variable and Nutrient-Dependent Efficiency. Stem Cells Dayt Ohio. 2018 Oct;36(10):1535–51.
9. Quadrato G, Nguyen T, Macosko EZ, Sherwood JL, Min Yang S, Berger DR, et al. Cell diversity and network dynamics in photosensitive human brain organoids. Nature. 2017 May;545(7652):48–53.
10. Saha A, Capowski E, Fernandez Zepeda MA, Nelson EC, Gamm DM, Sinha R. Cone photoreceptors in human stem cell-derived retinal organoids demonstrate intrinsic light responses that mimic those of primate fovea. Cell Stem Cell. 2022 Mar 3;29(3):460-471.e3.
11. O'Hara-Wright M, Gonzalez-Cordero A. Retinal organoids: a window into human retinal development. Dev Camb Engl. 2020 Dec 24;147(24):dev189746.

12. Salbaum KA, Shelton ER, Serwane F. Retina organoids: Window into the biophysics of neuronal systems. Biophys Rev. 2022 Jan 18;3(1):011302.
13. Bell CM, Zack DJ, Berlinicke CA. Human Organoids for the Study of Retinal Development and Disease. Annu Rev Vis Sci. 2020 Sep 15;6:91–114.
14. Zhang H, Bussmann J, Huhnke FH, Devoldere J, Minnaert A, Jiskoot W, et al. Together is Better: mRNA Co-Encapsulation in Lipoplexes is Required to Obtain Ratiometric Co-Delivery and Protein Expression on the Single Cell Level. Adv Sci. 2022 Feb;9(4):2102072.
15. Achberger K, Cipriano M, Düchs MJ, Schön C, Michelfelder S, Stierstorfer B, et al. Human stem cell-based retina on chip as new translational model for validation of AAV retinal gene therapy vectors. Stem Cell Rep. 2021 Sep 14;16(9):2242–56.
16. Völkner M, Pavlou M, Büning H, Michalakis S, Karl MO. Optimized Adeno-Associated Virus Vectors for Efficient Transduction of Human Retinal Organoids. Hum Gene Ther. 2021 Jul;32(13–14):694–706.
17. Garita-Hernandez M, Routet F, Guibbal L, Khabou H, Toualbi L, Toualbi L, et al. AAV-Mediated Gene Delivery to 3D Retinal Organoids Derived from Human Induced Pluripotent Stem Cells. Int J Mol Sci. 2020;
18. Kruczek K, Swaroop A. Pluripotent stem cell-derived retinal organoids for disease modeling and development of therapies. Stem Cells Dayt Ohio. 2020 Oct 1;38(10):1206–15.
19. Muller A, Sullivan J, Schwarzer W, Wang M, Park-Windhol C, Klingler B, et al. High-efficiency base editing for Stargardt disease in mice, non-human primates, and human retina tissue. bioRxiv. 2023;
20. Jüttner J, Szabo A, Gross-Scherf B, Morikawa RK, Rompani SB, Hantz P, et al. Targeting neuronal and glial cell types with synthetic promoter AAVs in mice, non-human primates and humans. Nat Neurosci. 2019 Aug;22(8):1345–56.
21. Velicky P, Miguel E, Michalska JM, Lyudchik J, Wei D, Lin Z, et al. Dense 4D nanoscale reconstruction of living brain tissue. Nat Methods. 2023 Aug;20(8):1256–65.
22. Stringer C, Wang T, Michaelos M, Pachitariu M. Cellpose: a generalist algorithm for cellular segmentation. Nat Methods. 2021 Jan;18(1):100–6.
23. Au HKE, Isalan M, Mielcarek M. Gene Therapy Advances: A Meta-Analysis of AAV Usage in Clinical Settings. Front Med. 2022 Feb 9;8:809118.
24. Pavlou M, Schön C, Occelli LM, Rossi A, Meumann N, Boyd RF, et al. Novel AAV capsids for intravitreal gene therapy of photoreceptor disorders. EMBO Mol Med. 2021 Apr 9;13(4):e13392.
25. Eiraku M, Takata N, Ishibashi H, Kawada M, Sakakura E, Okuda S, et al. Self-organizing optic-cup morphogenesis in three-dimensional culture. Nature. 2011;
26. Kretzmann JA, Liedl A, Monferrer A, Mykhailiuk V, Beerkens S, Dietz H. Gene-encoding DNA origami for mammalian cell expression. Nat Commun. 2023 Feb 23;14(1):1017.
27. Yu J, Vodyanik MA, Smuga-Otto K, Antosiewicz-Bourget J, Frane JL, Tian S, et al. Induced pluripotent stem cell lines derived from human somatic cells. Science. 2007 Dec 21;318(5858):1917–20.
28. Becirovic E, Böhm S, Nguyen ONP, Riedmayr LM, Hammelmann V, Schön C, et al. AAV Vectors for FRET-Based Analysis of Protein-Protein Interactions in Photoreceptor Outer Segments. Front Neurosci. 2016;10:356.
29. Hacker UT, Wingenfeld L, Kofler DM, Schuhmann NK, Lutz S, Herold T, et al. Adeno-associated virus serotypes 1 to 5 mediated tumor cell directed gene transfer and improvement of transduction efficiency. J Gene Med. 2005 Nov;7(11):1429–38.

Acknowledgements

We thank Sebastian Willenberg and Guillermo Prol Castello for their contributions in the segmentation software. This work was supported by the European Research Council (ERC) under the European Union's Horizon 2020 research and innovation program (Grant Agreement No. 850691), the Center for NanoScience (CeNS) at the Ludwig-Maximilian-University (LMU) Munich and the Munich Cluster for Systems Neurology (SyNergy). In addition, it was supported by the Deutsche Forschungsgemeinschaft (DFG, German Research Foundation) – Forschergruppe Project number 513025799.

Author contributions

S.M., F.S. and K.S. conceived the research. K.S. and S.S. cultured the human organoids, R.J. and T.S.R. the mouse organoids. K.S., T.S.R. and F.S. developed the analysis pipeline. T.S.R. analyzed the data. S.B. and S.M. prepared the AAVs. K.S. performed transduction experiments. Confocal imaging was performed by K.S. and S.S. (human organoids) and R.J. and T.S.R. (mouse organoids). Immunohistochemistry was performed by K.S. and S.S.. E.S. performed statistical analysis. All authors contributed to the manuscript.

Declaration of Interests

S.M. is cofounder of the gene therapy company, ViGeneron GmbH, who owns the rights on the related patent application WO/2019/076856 covering the AAV2.NN and AAV9.NN. All other authors declare no competing interests.

Supplementary Information

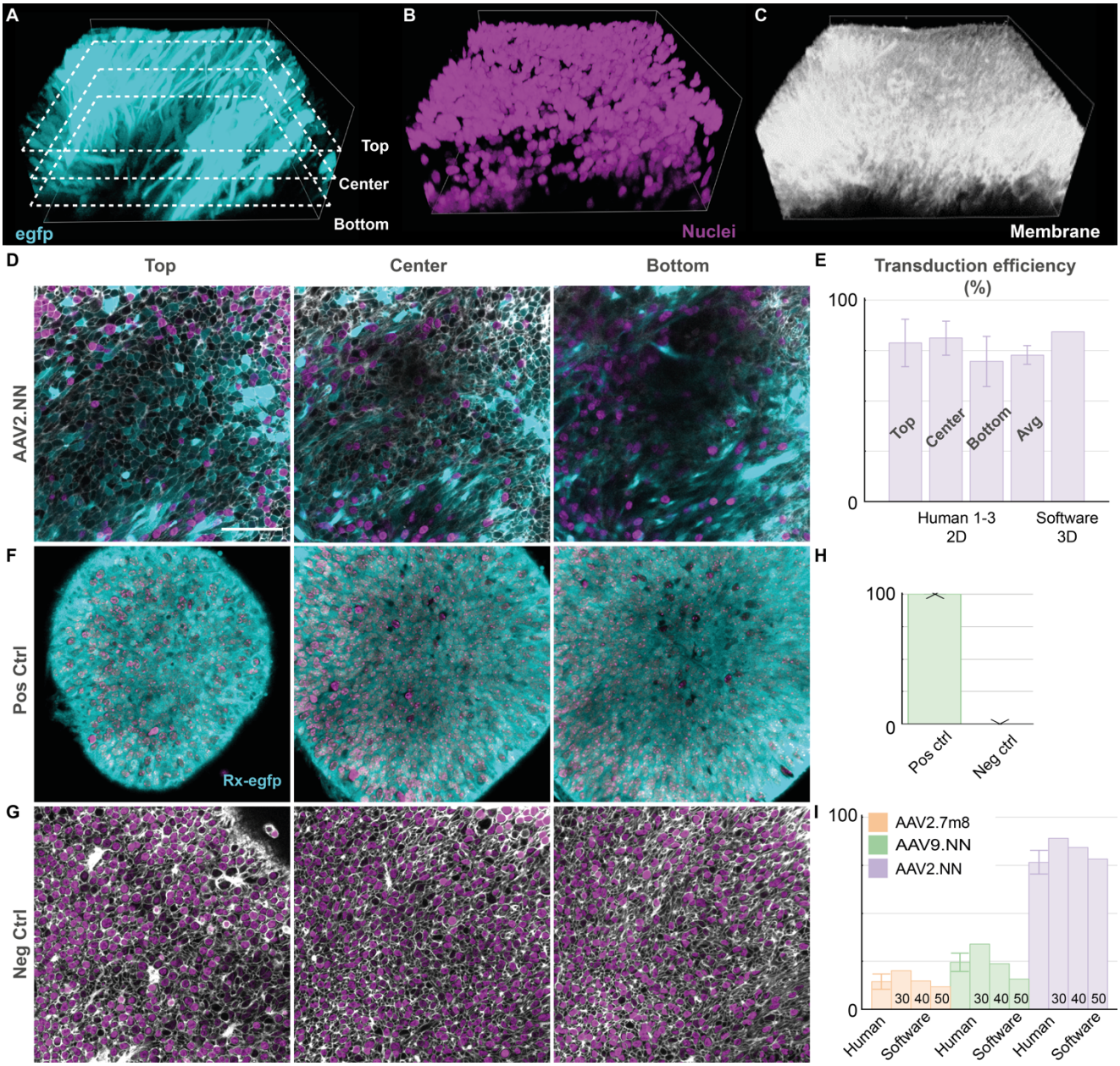

Supplementary Figure S1: Assessment of analysis pipeline and comparison with human counting. (A-C) 3D maximum intensity rendering of a confocal microscopy stack of a 239 days old human retinal organoid transduced with AAV2.NN. (D) 2D planes from data (A-C) at different positions allow manual assessment of transduced and total number of cells. (E) Transduction efficiencies of images in (D) quantified via 3 human annotators. The efficiency for human annotation (3 annotators) averaged over the three planes (top, center, bottom) yields (73 ± 5) % (mean ± std) compared to 84 % for the software. (F) Confocal images of an 18 days old mouse retinal organoid expressing egfp under the rx-promotor. (G) Confocal images of a 264 days old human retinal organoid without virus. (H) Quantification of transduction efficiency for positive (F) and negative (G) control. (I) Comparison of transduction efficiencies as a function of shell volume threshold (see main text) and human annotation for three organoids transduced with different AAVs. Scale bar: 50 microns. Error bars indicate the standard deviation (SD).

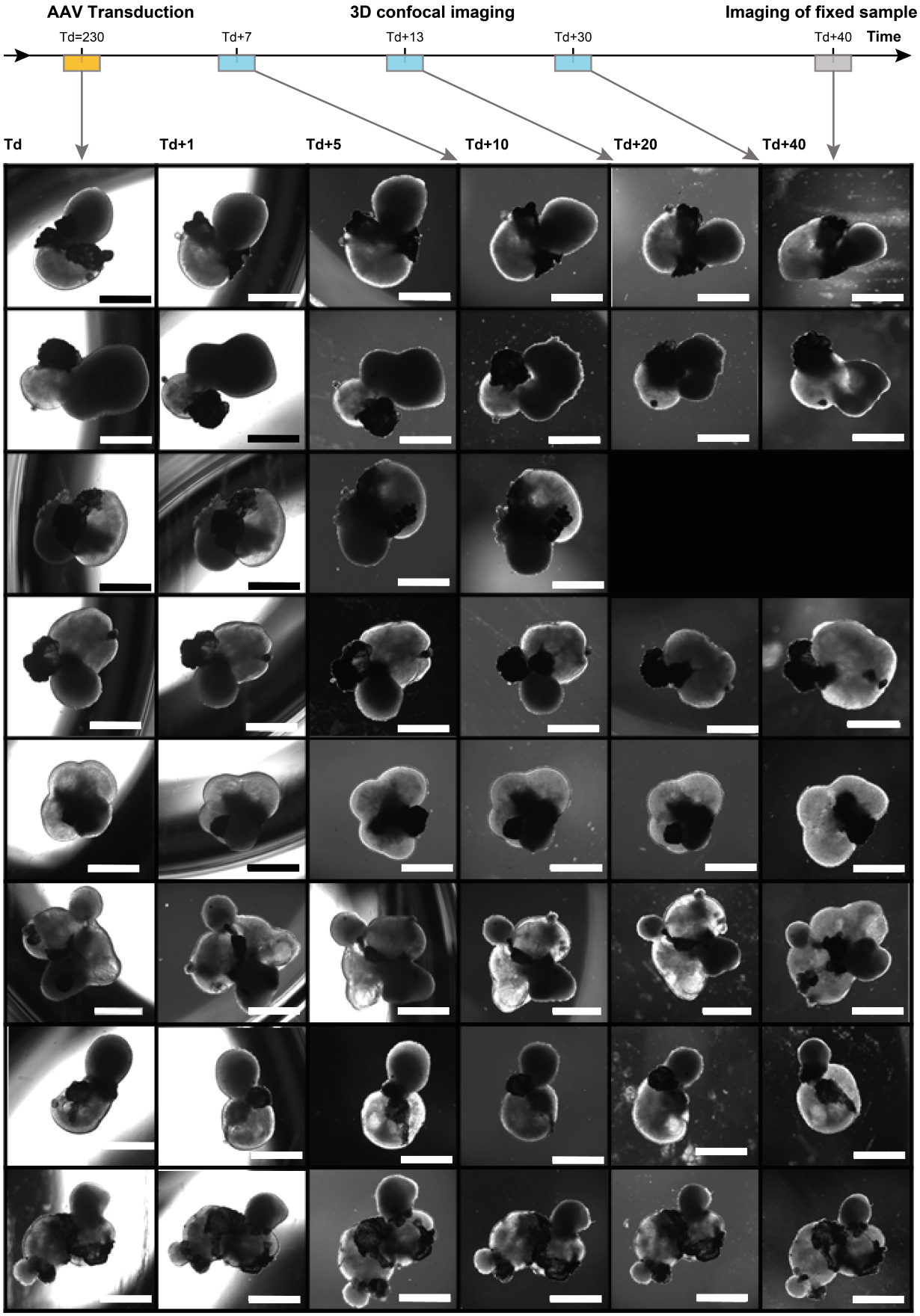

Supplementary Figure S2. Brightfield images of 8 human retinal organoids transduced with AAV2.7m8 and imaged at six time points after transduction (Td), related to Figure 4. Organoids from transduction experiment T1-8 from top to bottom. T1 was transduced at DIV227, T8 at DIV235. Scale bars: 500 microns.

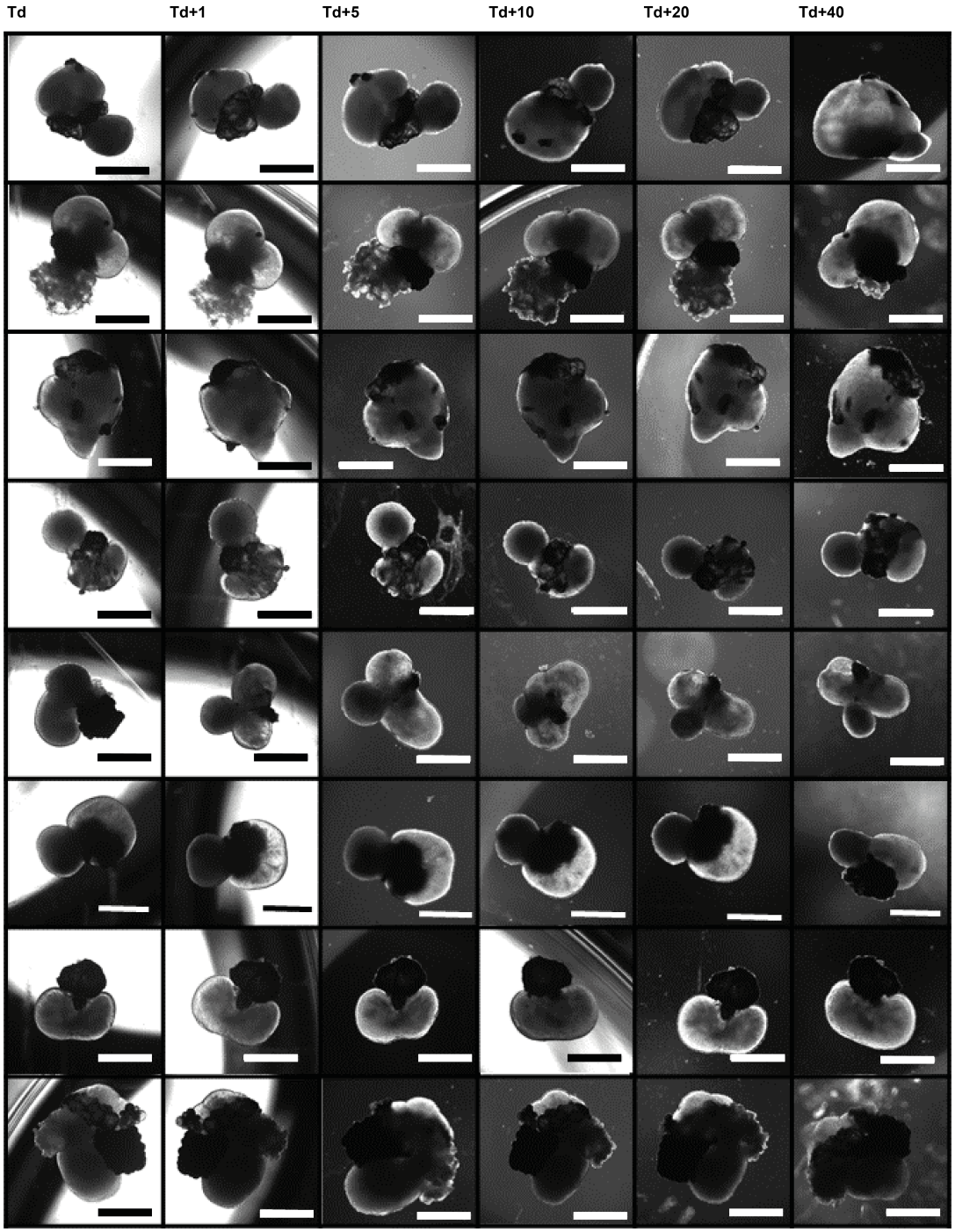

Supplementary Figure S3. Brightfield images of 8 human retinal organoids transduced with AAV9.NN and imaged at six time points after transduction (Td), related to Figure 4. Organoids from transduction experiment T1-8 from top to bottom. T1 was transduced at DIV227, T8 at DIV235. Scale bars: 500 microns.

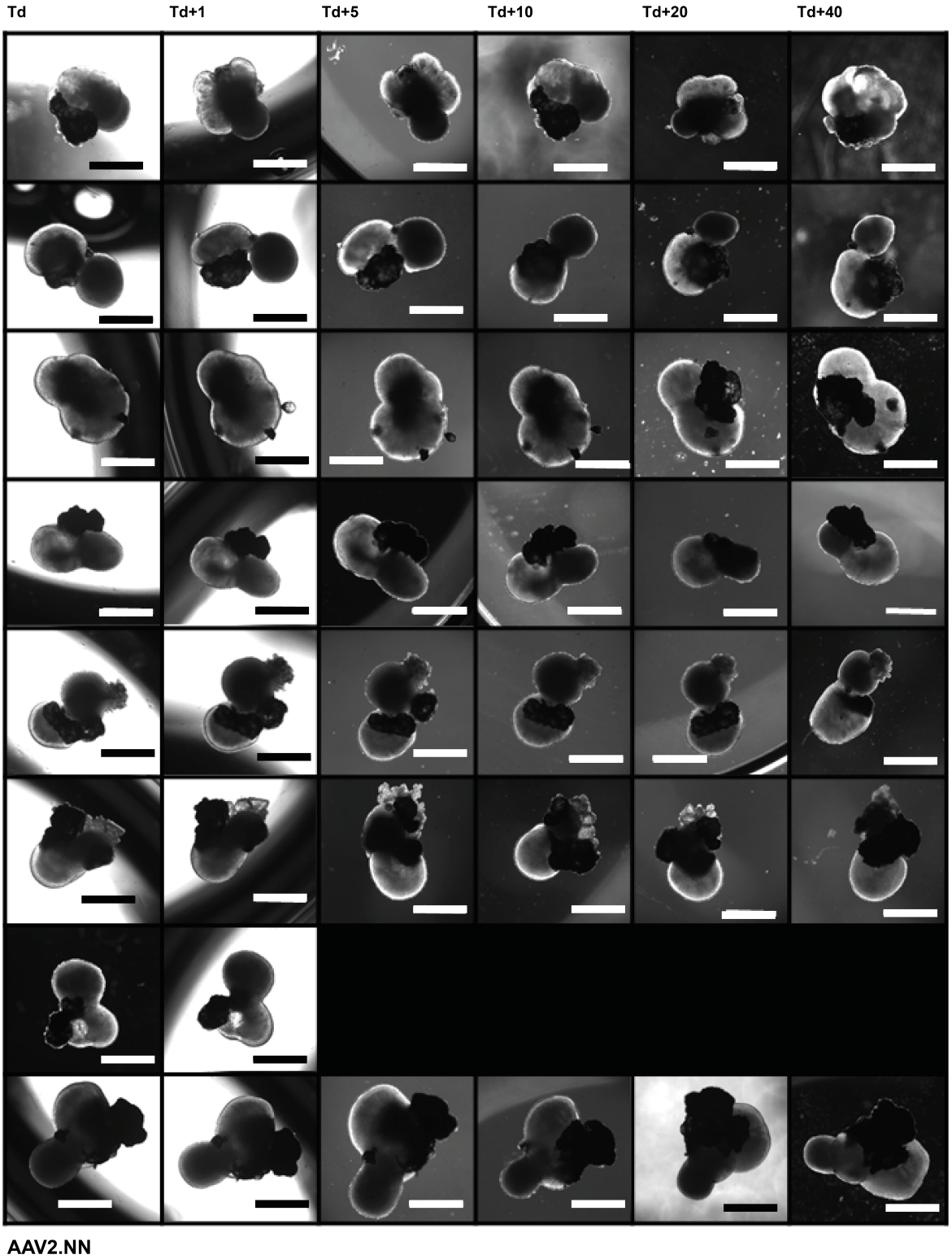

Supplementary Figure S4. Brightfield images of 8 human retinal organoids transduced with AAV2.NN and imaged at six time points after transduction (Td), related to Figure 4. Organoids from transduction experiment T1-8 from top to bottom. T1 was transduced at DIV227, T8 at DIV235. Scale bars: 500 microns.

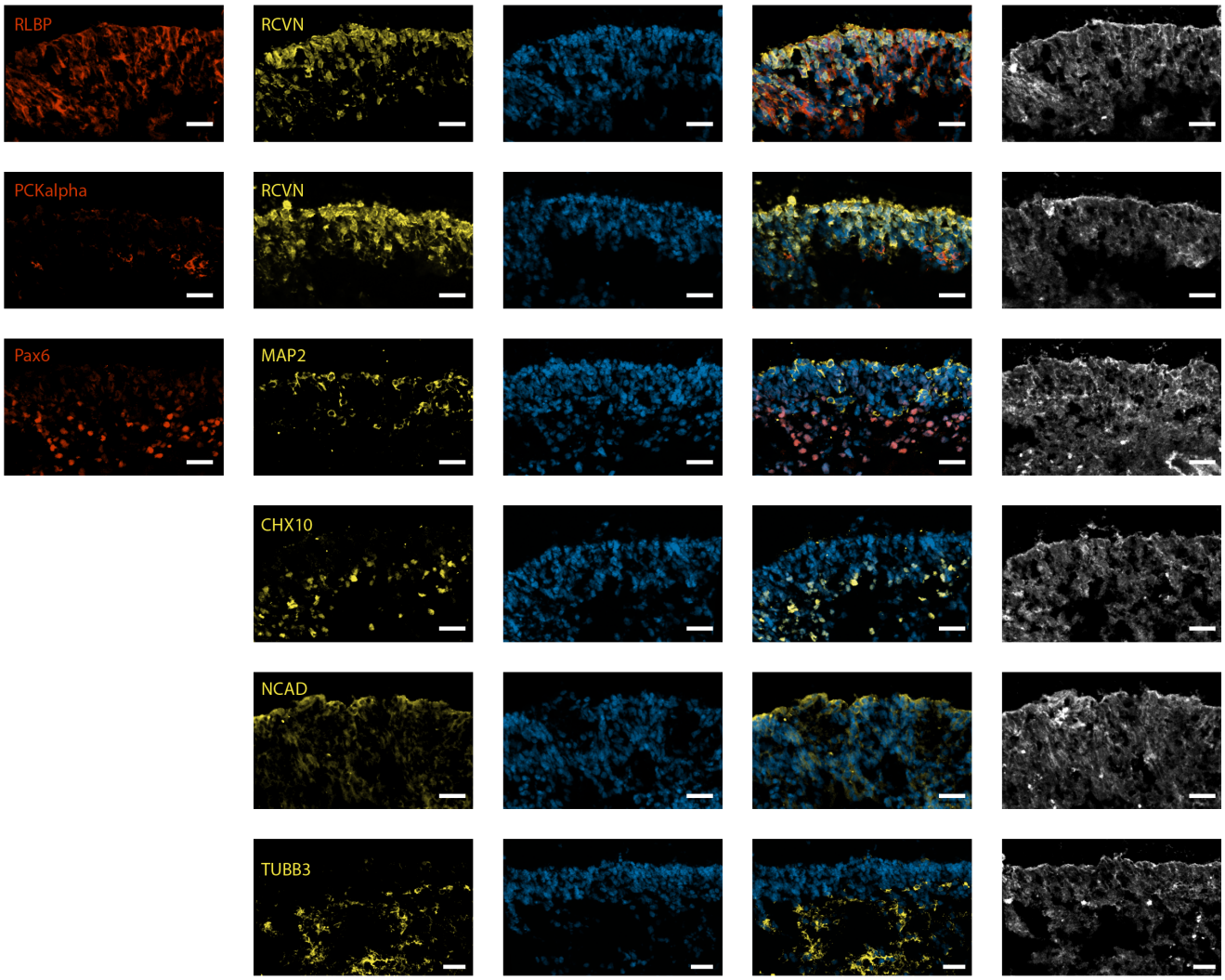

Supplementary Figure S5. Confocal images of immunofluorescence staining DIV227 human retinal organoids. Primary antibodies indicated in red and yellow, blue: DAPI, white: WGA-CF membrane stain. Scale bar: 30 microns.

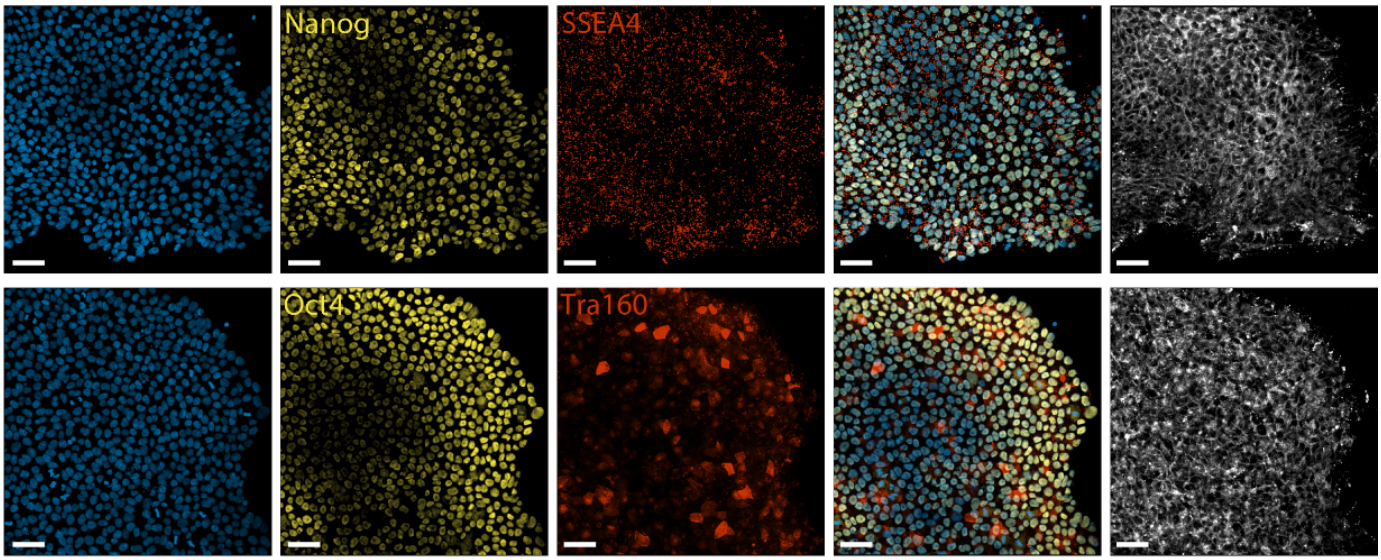

Supplementary Figure S6. Confocal images of pluripotency staining of iPS(IMR90)-4p37. Primary antibodies indicated in yellow and red, blue: DAPI, white: WGA-CF membrane stain. Scale: 50 microns.

RESOURCE AVAILABILITY

Lead contact

Further information and requests for resources and reagents should be directed to and will be fulfilled by the lead contact, Friedhelm Serwane (f.serwane@lmu.de).

Materials availability statement

- No plasmids were generated in this study.

Data and code availability

- Microscopy data reported in this paper will be shared by the lead contact upon request.
- Any additional information required to reanalyze the data reported in this paper is available from the lead contact upon request.

EXPERIMENTAL MODEL AND STUDY PARTICIPANT DETAILS

Human induced pluripotent stem cells from a female donor iPS(IMR90)-4 (WiCell®, (27)) were used from this study. The cell line and the corresponding organoids were cultured at 37° and 5% CO_2.

METHOD DETAILS

Human iPSC culture

The commercially available cell line iPS(IMR90)-4 (WiCell®, (27)) was cultured according to WiCell® protocol. Matrigel was prepared by dissolving 1.0 mg Matrigel (Corning® Matrigel® Basement Membrane Matrix Growth Factor Reduced, 354230, lot number: 0295001) with 1 ml cold DMEM/F-12 medium (Glutamax, GIBCO, 31331-028). The dissolved Matrigel solution was further diluted with the addition of 11 ml cold DMEM/F-12 medium. 1 ml of diluted Matrigel solution was plated per well in a 6-well plate which was then

incubated at 37°C for 1-2 hours. Once the Matrigel set, 1 ml DMEM/F-12 medium was added to each well to prevent drying. Plates were kept at 37°C overnight.

IPSCs were thawed in a 37°C water bath and subsequently diluted with mTeSR1 medium (Stem Cell Technologies, 85850). The cells were centrifuged at 200g for 5 minutes, supernatant was discarded, and the cells were resuspended in mTeSR1 medium (0.5 ml/well to be seeded) supplemented with 10µM Rock Inhibitor (Stem Cell Technologies, Y-27632) for every 6-well that should receive cells. Medium removed from the prepared Matrigel coated wells and 0.5 ml of cells were plated per well. The iPSCs were moved to the incubator (37°C) and were fed with 2 ml culture medium daily. Once the colonies became too dense or increased differentiation occurred, the iPSCs were passaged.
Passaging (1:2 ratio) was conducted using EDTA (Sigma-Aldrich, E8008) as described in the WiCell® protocol. Areas containing differentiated cells were removed manually using a pipette tip under a stereomicroscope. Media was aspirated from each well and wells were subsequently rinsed with 1 ml PBS (Dulbecco, Biochrom, L182-50). PBS was then aspirated from each well. To remove the iPSCs from the surface of the well, 1 ml EDTA was added at RT and incubated for 6-9 minutes. Meanwhile, new culturing dishes were prepared by replacing the medium in new Matrigel coated wells with 1 ml of mTeSR1 medium/well. Following the incubation period, EDTA was aspirated and the cells were detached gently from the surface using 2 ml culture medium and a pasteur pipette. 1 ml of homogenous cell colonies were plated onto each new Matrigel coated well, distributed evenly by slight movement of the dish, and incubated overnight.

Human retinal organoid culture

hROs were generated in agarose microwell arrays which restrict the size of growing organoids following the protocol described in Cowan et al with minor alterations. This method has been found to efficiently generate organoids while requiring less iPSCs than alternative approaches (6).
Agarose molds were prepared for iPSC culture. MicroTissues® 3D Petri Dish® micro-mold spheroids (Sigma, Z784019) were filled with 2% agarose (Thermo Fisher Scientific, R0491) dissolved in DMEM (Thermo Fisher Scientific, 10569-010). The solidified agarose molds were transferred into a 12-well dish. The molds were equilibrated by adding 1.5 ml mTeSR1 medium was added to each well and the plates were incubated at 37°C for a minimum of 15 minutes. This equilibration step was repeated with fresh mTeSR1 medium. The molds were stored at 4°C and a final equilibration was done with fresh mTeSR1 media.

Before seeding iPSCs into the microwells, the cells were plated and passaged once in a Matrigel coated 6-well plate as described above. To dissociate the iPSCs from the 6-well plate, each well was washed twice with 1 ml PBS and incubated for 10 minutes in 600 µl PBS + 0.5 M EDTA at room temperature. After aspirating the PBS + EDTA, the plate was incubated in 500 µl Accutase (Invitrogen, 00-4555-56) for 3 minutes at 37°C. 1 ml mTeSR1 + 10 µM RI was added and the cells were pipetted up and down to generate a single cell suspension. Cells were pelleted for 5 minutes at 200g, supernatant was discarded, and the cells were resuspended in 5 ml mTeSR1 + 10 µM RI. To seed, the cells were diluted to achieve a concentration of approximately 60,000 cells in 150 µl and 150 µl are seeded per agarose well. To allow the cells to settle, the plate was placed in the incubator (37°C) for 30 minutes, after which the well was filled up with 1.5 ml mTeSR1 + 10 µM RI. The plates were kept in the incubator at 37°C and fed according to the following.

On day 1, a third of the medium was replaced with NIM medium containing DMEM/F12, N2 supplement (GIBCO, 17502-048), 1% non-essential amino acid (NEAA) solution (SIGMA, M7145), and 2 µg/ml Heparin (SIGMA, H3149). On day 2, half of the medium was replaced with NIM medium and on day 3, the entire medium was replaced with NIM medium. From day 4 to day 6, 1.5 ml NIM medium were added daily.
On day 7, the embryoid bodies were transferred to a Matrigel coated 6-well plate and the NIM medium was replaced daily.

From day 16 on, NIM medium was replaced with 3:1 medium containing 72% DMEM (GIBCO, 10569-010), 24% F12 (GIBCO, 31765-027), 2% B27 w/o VitA (GIBCO, 12587-010), 1% NEAA (Sigma, M7145), and 1% Pen/Strep (GIBCO, 15140-122). The medium was replaced daily.
On day 31, retinal structures were detached by checkerboard scraping scratching a 1-2 mm grid with a 200 µl pipette tip. This causes retina structures to come off in larger tissue pieces. Debris and single cells were removed by washing the aggregates three times in a 15 ml tube in 3:1 medium by sedimentation. The aggregates were maintained in suspension in 6-7 ml 3:1 medium in 6 cm plates. The media of the floating cultures was changed three times per week.
One week after checkerboard scraping on day 38, aggregates that did not contain phase-bright stratified neuroepithelium were manually removed.
From day 42, the 3:1 medium was supplemented with 10% heat-inactivated FBS (Sigma-Aldrich, ES009-B) and 100 µM taurine (T0625-25G, dissolved in MiliQ H2O). Organoids were fed three times a week.
After day 70, the aforementioned 3:1 medium supplemented with FBS and taurine was further supplemented with 1 µM retinoic acid (Sigma, R2625, dissolved in DMSO).
From day 98 on, the B27 supplement in the 3:1 medium was replaced with N2 supplement (GIBCO, 17502-001) and retinoic acid was reduced to 0.5 µM.

Fixation: Retina organoids were fixed in 4% PFA (Sigma-Aldrich, F8775-25ML) in PBS overnight at 4°C. Afterwards, the organoids were cryopreserved in PBS containing 30% sucrose (Sigma, S1888-500G) overnight at 4°C. For the fixed TP4 measurements, organoids where incubated for 48 hours in PBS, 0.5% Triton and stained with DAPI and 1:500 WGA-CF (Supplementary Table 1).

Cryosectioning: 2-4 organoids were embedded in Neg-50™ Frozen Section Medium (Thermo Fisher Scientific, 6502B) and frozen on dry ice. Cryosections (10 µm) were cut using a Epredia™ CryoStar™ NX70 cryostat. The slices were picked up directly with SuperFrost Plus™ Adhesion slides (Epredia™ J1800AMNZ). The slides were left at RT to dry for at least 2h and stored at -80°C.

Staining: Slides were left at RT to thaw and dry for 30 minutes and rehydrated in PBS until the embedding medium was dissolved and only the organoids remained on the slides. The sections were incubated in blocking solution containing PBS, 0.5% Triton X-100 (Roth, 3051.3), and 1% BSA (Sigma, A7638-10G) for 1h at RT.
The blocking solution was aspirated and primary antibodies (Supplementary Table 1) diluted in blocking solution were added to the slides and incubated overnight at 4°C. Slides were rinsed in PBS for ten minutes twice. Secondary antibodies diluted in blocking solution, DAPI, and the membrane stain WGA CF555 were added to the slices and incubated for 2 hours at RT. Slides were rinsed in PBS for ten minutes twice and subsequently rinsed once more in distilled water. Coverslips were mounted to the slides using Mounting Medium Fluoromount-G™ (Thermo Fisher Scientific, 00-4958-02).

AAV vector production

AAV vector production was performed as previously described (24,28). A self-complementary AAV plasmid containing a cytomegalovirus-enhanced green fluorescent protein (CMV-eGFP) expression cassette flanked by ITRs from AAV2 (29) was used as the vector genome plasmid.

Transduction experiments

Per condition, eight organoids were transduced, with the first transduction (T1) taking place at DIV227. The procedure was repeated daily until DIV 235 with one organoid per condition per day. At the day of transduction (Dt), 5*10^10 viral genomes/organoid were added, and the viral solution was filled up to 300 µl with culture media. On Dt+1 (one day after dT) the organoids were transferred into the wells of a 24-well plate. Each well

was filled up to 1ml with medium. On Dt+4, the organoid was washed twice with PBS and supplied with 1 ml fresh media. Then the organoids were integrated into the regular feeding schedule of three weekly exchanges of half the volume with fresh media. After imaging of Dt+30 the media was replaced completely with fresh media.

Organoid staining for live imaging

Nuclei were stained using Nuncspot Live 650 (Biotium, 1:250). Membranes were fluorescently labeled using CellBrite Steady 550 (Biotium, 1:1000). To this end, organoids in were placed in glass-bottom dishes, the stains were added to the medium and organoids were incubated at 37° for 2 hours. Organoids were imaged using a confocal microscope (LSM980, Zeiss) in combination with a water immersion objective (40x). The membrane channel was used as a guide to identify the retinal tissue within the organoid which was then exclusively imaged. Volumes which contained other tissue types such as RPE were discarded. A sampling of (1024x1024x400) voxel was chosen corresponding to an observation volume of (211x211x100) microns^3.

Analysis pipeline

In order to extract transduction efficiency information from the confocal 3D images, both the segmentation of the nuclei channel and the cytoplasmic eGFP expressing cells was obtained. The segmentation was performed using the Arivis Vision4D (Zeiss) software package in several steps:

1. Conversion of the raw images (1024x1024x400) voxel into the arivis .sis format.
2. Denoising of the channels using the Denoise option
3. Nuclei segmentation via Cellpose (22) interfaced via python. For the cellpose segmentation following settings were used:
    a. Binning to 50%
    b. Discrete Gaussian denoising (0.829 µm diameter)
    c. Cellpose custom model: CPx (Cellpose 2.0)
    d. Thresholds: estimated diameter in µm: 5.0; flow threshold: 1.0, Mask inclusion threshold (cellprob. threshold): -6; maximal tile size: 4096 pixels, nuclei object volume filter [10 µm^3, 1 m^3]
4. Segmentation of the transduced volume (cytoplasmic eGFP) via the Arivis Machine Learning trainer. Settings were:
    a. Arivis Machine Learning probability training for segmentation (trained on microscopy images of organoids to recognize areas with fluorescence signal as transduced and the background as not transduced)
    b. Intensity threshold segmentation: Set range to exclude probabilities lower than 50%
    c. Set object threshold: Only objects larger than 10 µm^3
5. Identification of nuclei of transduced cells (nuclei that are located within a transduced environment):
    a. Set Nuclei size threshold to larger than 100 µm^3
    b. Dilated nuclei objects by 2 pixels
    c. To obtain the virtual shell around the nuclei subtracted intersection calculation (A-B) between the dilated nuclei objects (A) and the non-dilated nuclei objects (B)
    d. Removed artifacts by applying a threshold of 50 µm^3 (human organoid tissue; 30 µm^3 for mouse organoid tissue) minimal size to the shells (determinable by the ratio between the number of nuclei to the number of shells (≈ 1))
    e. Calculated compartments of the transduced volume segmentation to the size filtered shells (overlap threshold > 40%). The threshold is determined as shown in Suppl. Fig. S1.
    f. To obtain nuclei of transduced cells: Filter shells by overlap ≥ 0.4 (depending on threshold chosen for step e.)

g. Export summary for the total nuclei count (size filtered shells) and the number of transduced nuclei (shells with overlap ≥ 0.4)
h. Obtain transduction efficiency by dividing the sum of shells with overlap ≥ 0.4 by the sum of size filtered shells

Comparison with human counting

One confocal image stack taken at Td+7 was selected for each AAV serotype. Three planes were extracted from each stack at the heights of 25 µm, 50 µm and 75 µm (total stack height: 100 µm, Supplementary Figure S1). The total cell number and the number of transduced cells were then independently counted by three humans using the AAV2.NN sample. The manual counting was based on the membrane label and the fluorescence signal from the AAV-delivered eGFP and performed using ImageJ. Both cells with low and high fluorescence were counted as transduced. Based on the comparison of the average human result with the pipeline, a suitable shell threshold for the pipeline was established (40%). In a final step, the selected threshold was tested by comparing the result of two other image sets (AAV2.7m8, AAV9.NN) with human annotation.

QUANTIFICATION AND STATISTICAL ANALYSIS

Statistical details of the experiments can be found in the figure captions, including the number of biological samples (organoids) and the type of error bars. For the statistical analysis used Figure 4 the software package Origin was used. A Two-Sample t-test was used to calculate p-values assuming equal variances.

ADDITIONAL RESOURCES

N.A.

Supplementary Table 1. Antibodies used for live imaging, staining of cryosectioned organoids, and pluripotency staining of iPSCs.

Antibody	Manufacturer	Product number	Dilution (Concentration)
Recoverin	Sigma	AB5585	500
RLBP1/CRALBP	abcam	AB15051	100
RBPMS	PhosphoSolutions	1830-RBPMS	100
RBPMS-thermo	Thermo Fisher Scientific	PA5-31231	100
Tuj1	Biolegend	801213	100
PCKalpha	Santa Cruz Biotechnology	sc-8393	100
n-Cadherin	Thermo Fisher Scientific	PA5-29570	200
Rx	Santa Cruz Biotechnology	sc-271889	200
MAP2 aves	Aves labs	MAP-0020	500
Pax6	GeneTex	GTX113241	100
ZO-1	Thermo Fisher Scientific	40-2200	100
CHX10	Thermo Fisher Scientific	PA1-12565	200

Nanog	Gift from D. Paquet		500
Oct4	Gift from D. Paquet		500
SSEA4	Gift from D. Paquet		100
Tra160	Gift from D. Paquet		500
DAPI	Invitrogen	D1306	(0.1 µg/ml)
WGA CF 555	Biotium	29076	1000
Goat anti-Rabbit IgG (H+L) Cross-Adsorbed Secondary Antibody, Alexa Fluor 488	Invitrogen	A-11008	500
Goat anti-Chicken IgY (H+L) Secondary Antibody, Alexa Fluor 488	Invitrogen	A-11039	500
Goat anti-Mouse IgG (H+L) Cross-Adsorbed Secondary Antibody, Alexa Flour 647	Invitrogen	A-21235	500
Goat anti-Rabbit IgG (H+L) Cross-Adsorbed Secondary Antibody, Alexa Fluor 647	Invitrogen	A-21244	500
Donkey anti-Sheep IgG (H+L) Cross-Adsorbed Secondary Antibody, Alexa Fluor 647	Invitrogen	A-21448	500
NucSpot Live 650 Nuclear Stain	Biotium	40082-T	250
Cellbrite steady 550 membrane	Biotium	30107-T	1000